Maximum precipitation altitude on the northern flank of the Qilian Mountains, northwest China

Rengsheng Chen, Chuntan Han, Junfeng Liu, Yong Yang, Zhangwen Liu, Lei Wang and Ersi Kang

ABSTRACT

Investigation of the altitude of maximum precipitation (AMP) and the factors that determine this height supports the understanding of vertical precipitation distribution in mountains. Based on the field precipitation measurement on the northern flank of the Qilian Mountains, the AMP was investigated at vertical profiles from 1,483 to 4,484 m. It found a 2,300 m-AMP in winter and a 4,200 m-AMP in other seasons and on a yearly scale. The AMPs increase from the cold and dry season to the warm and wet season and therefore increase with precipitation. During winter, the interaction of the predominant high-pressure system, the thermal inversion layer below 2,200 m, and the westerly lead to the 2,300-m AMP. In other seasons, the convergent Tibetan Plateau monsoon causes the water vapor move to the Qilian Mountains, and the enhanced uplifting by the mountain produces greater precipitation with altitude, forming the AMP at the higher areas. The front steepest terrain is the primary factor causing the formation of 4,200-m AMP in the study area. The annual AMP may be roughly equal to seven-eighths of the altitude of the mountain top on the north flank of the Qilian Mountains.

Key words | maximum precipitation altitude, mechanisms, Qilian Mountains, seasonal variation

Rengsheng Chen (corresponding author)
Chuntan Han
Junfeng Liu
Yong Yang
Zhangwen Liu
Lei Wang
Ersi Kang
Qilian Alpine Ecology and Hydrology Research Station, Key Laboratory of Ecohydrology of Inland River Basin, Northwest Institute of Eco-Environment and Resources,
Chinese Academy of Sciences,
Lanzhou 730000,
China
E-mail: *crs2008@lzb.ac.cn*

INTRODUCTION

Accurate areal precipitation data are important for hydrology, agriculture, ecosystem, and other subjects, but gathering such data is very difficult due to the varied spatial and temporal distribution features of precipitation and the lack of effective measurement techniques in mountainous areas. In alpine areas with complex topography and a large altitude range, the usual precipitation data from satellite remote sensing and general circulation models (GCMs) with low spatial resolution do not reveal the varied precipitation distribution features. Furthermore, the mountain precipitation is often much lower when estimated by satellite remote sensing such as GPM IMERG (Integrated Multi-satellitE Retrievals for Global Precipitation Measurements) and TRMM (Tropical Rainfall Measuring Mission satellite) (Xu *et al.* 2017) and higher when estimated by GCMs (Mueller & Seneviratne 2014) in western China. Ground-based radar is also limited by the complex terrain, and the gauges are often limited by the density and representativeness of their placement, especially the paucity of high-altitude stations in alpine areas. Therefore, it is important to study the influence of mountain barriers on the amount and distribution of precipitation and to consider basic condensation processes and the ways that mountains can affect cloud and precipitation regimes (Barry 2008).

Considerable attention has been devoted in recent decades to studies of precipitation mechanisms and orographic effects on precipitation amounts and their spatial distribution. As more data have been collected and the

doi: 10.2166/nh.2018.121

methods used in large mountain ranges have been reported (e.g., Aizen *et al.* 1996; Thomas 1997; Sevruk & Nevenic 1998; Rubel & Rudolf 2001; Sevruk & Mieglitz 2002; Putkonen 2004; Ahrens 2006; Prat & Barros 2010; Wulf *et al.* 2010; Akkiraz *et al.* 2011), many aspects of the basic mechanisms of orographic precipitation have been explained (Roe 2005; Barry 2008). However, some important issues remain unresolved because of the lack of data from higher mountainous regions (Marquínez *et al.* 2003; Roe 2005; Ward *et al.* 2011). One debated issue regards the altitudes of maximum precipitation (AMPs) in a mountain's vertical precipitation profile, especially in alpine areas with complex topography and few gauges. In a mountain's vertical precipitation profile, the maximum precipitation should exist according to the theory of atmospheric boundary layer physics. The altitude of this maximum on a precipitation–altitude curve is called the AMP. Precipitation increases with altitude below the AMP but decreases with altitude above the AMP; therefore, determining the AMP is beneficial for understanding the moisture movement, condensation, and vertical precipitation distribution of a mountain. Hence, it is also an important input of some hydrological models (e.g., Xu & Singh 1998; Gao *et al.* 2012, 2017).

The AMP has been studied for several decades, especially from the 1960s to the 1990s. In 1976, Lauscher divided AMPs into five types using global data collected from 1,300 stations, but only 3.3% of the stations concerned lay over 2,000 m above sea level. The five types are T (tropical), E (equatorial), Tr (transitional), M (mid-latitude), and P (polar), and have been revised in more recent work (Barry 2008). In the early years, according to the theory of the atmospheric boundary layer physics, the moisture content in mid-latitude mountains would decrease and condensation would be reduced above the AMP, leading to lower precipitation in the higher regions. Therefore, there should only be one AMP, which would appear at the foot or at the middle of the mountain (e.g., Sarker 1966; Rumney 1968; Shen 1975; Lauscher 1976; Li 1976, 1982; Barry 1981). Considering factors such as the prevailing wind direction, slope, aspect, elevation, and climate in the mountains, several analytical and empirical models have also been created to describe the moisture condensation and the effects of mountain barriers to precipitation (e.g., Ding & Kang 1985; Alpert 1986; Zhang & Deng 1987; Fu 1992). In most low and mid-sized mountains, the one-AMP theory and the model results are verified by the measurements. In some alpine areas, the model-estimated AMP is also consistent to a certain degree with the measured AMP from the precipitation–altitude curve. For example, the estimated AMP in the northern Tien Mountains is about 2,100 m (Zhang & Deng 1987), and the measured AMP is about 1,800 m (Yang *et al.* 1991, 2000). In the Qilian Mountains, the estimated AMP is about 3,000 m (Ding & Kang 1985), and the measured AMP is about 2,800 m (Tang 1985; Ding *et al.* 1999). However, most alpine areas have a paucity of high-altitude weather stations, so their precipitation–altitude curves are incomplete because they are plotted using limited gauge data in the relatively low regions (Lin 1995; Yang *et al.* 2000). The one-AMP theory was first called into question by glacier investigations that found deep snow cover – meaning more precipitation – in the glacial firn basin than at the AMP (e.g., Kou & Su 1981; Kotlyakov & Krenke 1982; Bai & Yu 1986). Limited field observations also indicated that there may be two or more AMPs in alpine areas. For example, in the northern Tien Mountains, two AMPs were found in 1987 in the source regions of the Urumqi River basin (Yang *et al.* 1991, 2000). One was at about 1,800 m with yearly precipitation of about 583.2 mm, and the other was located at the firn basin of Urumqi No. 1 glacier (4,030 m a.s.l.) with 650.2 mm precipitation. In the Himalayas, at least two AMPs have been found at the foot and between 2.0 and 2.4 km (Alpert 1986; Putkonen 2004). In the northern Qilian Mountains, Wang *et al.* (2009) also find another AMP (about 4,510 to 4,670 m) on the Qiyi glacier (97.5 °E, 39.5 °N) based on the measurements from August 10, 2007, to September 12, 2008. However, even in the same northern Qilian Mountains, Chang *et al.* (2002) reported different results based on measurements from 1986 to 1990 in the Sidalong area (99°31′ to 100°15′E, 38°14′ to 38°44′E). They found one AMP at about 3,650 m. Barry (2008) concluded that the effects of altitude on the vertical distribution of precipitation in mountain areas are highly variable in different geographical locations. Sufficient measurements, especially at higher elevations, would help to answer these effects in various alpine areas (Ding *et al.* 1999; Wang *et al.* 2009).

The authors carried out this experimental study of precipitation measurement and distribution for more than 10

years in the Qilian Mountains. The Qilian Mountains on the northeast side of the Tibetan Plateau, facing the arid area of northwest China, have relatively abundant precipitation and generate most of the water resources in the adjacent arid region. This paper presents analysis of the new high-elevation precipitation data and reveals the altitude distribution of precipitation, the variation of AMPs, and the influencing factors on the northern flank of the Qilian Mountains. The results favor research on mountainous hydrology, meteorology, climate, ecosystems, and cryosphere sciences, also of the extended application of water resources allocation in arid regions.

DATA AND METHODS

Study area

The Qilian Mountains are located at the northeastern edge of the Tibetan Plateau (Figure 1(a)). Three large inland rivers (the Shiyang, Hei, and Shule) originate from the northern Qilian Mountains and flow to the arid regions to the north. River discharge from the Qilian Mountains is the only water resource that can be allocated for industry and agriculture in the arid middle and downstream areas of these inland basins. Although the precipitation station density is the greatest among the alpine areas in western China and adjacent countries, there are not that many stations, and none of them is higher than 3,400 m in the northern Qilian Mountains, where the altitude ranges from about 1,800 to 5,808 m. Thus, a relatively narrow region with more precipitation gauges than in other areas is chosen as the study area (Figure 1(a)).

The study area is about 140×110 km, and its altitude ranges from about 1,400 to 4,800 m (Figure 1(b)), with a mean of about 3,370.5 m, and altitudinal zonations are shown in Figure 1(c). From altitudes of about 1,400 to 1,800 m, oases are scattered throughout the desert. Bare soil dominates between 1,800 and 2,300 m, and mountainous grassland and coniferous forests grow from about 2,300 to 3,200 m. Alpine meadow predominates from about 3,200 to 3,800 m, and moraine and talus areas are located above 3,800 m. The glacier termini lie at about 4,200 to 4,300 m and 4,400 to 4,500 m on northern and southern slopes, respectively (Figure 1(b)). The wet season generally lasts from mid-May to mid-September, and snow falls in almost every month except July at altitudes above 3,000 m in the study area.

Data and methods

To determine the AMP in the study area, precipitation measurements with six weighted rain and snow gauges (TRwS 204; Hulu-1 to Hulu-6) have been conducted since 2008 at about 2,980, 3,232, 3,382, 3,711, 4,166, and 4,484 m in the small Hulu watershed (Figure 1 and Table 1; Chen *et al.* 2014). Using these new precipitation data from higher gauges and peripheral precipitation data from five China Meteorological Administration (CMA) stations (Zhangye, Minle, Sunan, Qilian, and Yeniugou; Figure 1(b) and Table 1) in the lower regions, the precipitation–altitude curves were plotted to determine the AMP on monthly, seasonal, and yearly scales. The results are discussed with regard to factors such as the formation of orographic precipitation, the effects of the general circulation of the atmosphere, synoptic scale uplift, convective instability, local topography, and land cover.

It is widely recognized that snowfall observation errors can be large in high winds and that precipitation gauge measurements contain systematic errors caused mainly by wetting, evaporation loss, and wind-induced undercatch (Sugiura *et al.* 2003). Because the gauges at the five CMA stations are unshielded, Chinese standard precipitation gauges (CSPGs; Table 1) and the Hulu watershed is a TRwS 204 gauge around a single Alter shield (Chen *et al.* 2014), their observation errors differ (Goodison *et al.* 1998) and the measured precipitation data should be calibrated to determine the actual precipitation before using them to plot the precipitation–altitude curves.

The wetting loss by the CSPG per observation is 0.23 mm for rainfall measurements, 0.30 mm for snow, and 0.29 mm for mixed precipitation, based on the measurements in the Tien Mountains (Yang 1988; Yang *et al.* 1991). The CSPG's special funnel-and-container (a narrow mouth bottle) design reduces evaporation loss to near zero compared to other losses in the warm, rainy season (Ye *et al.* 2004). In winter, the evaporation loss is already low (0.10 to 0.20 mm/day) according to results from Finland

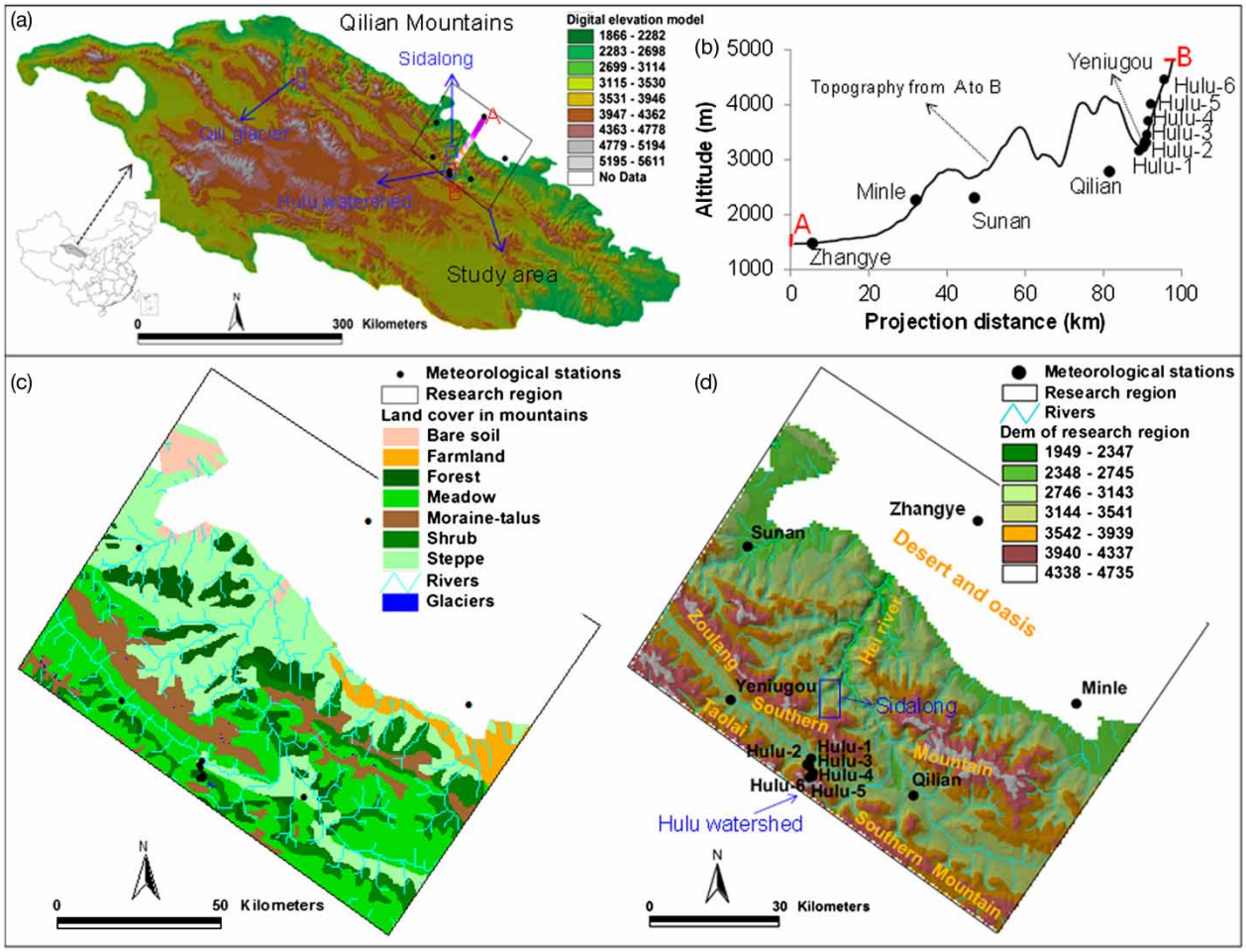

Figure 1 | Position (a), topography (b), land cover (c), and precipitation stations (d) in the study area.

Table 1 | Meteorological stations in the study area

No.	Name	Longitude	Latitude	Altitude (m)	Land cover	Gauge type	Gauge height (cm)	Orifice diameter (cm)
1	Zhangye	100°26′	38°56′	1,483	Farmland	Unshielded Chinese standard precipitation gauge (CSPG)	70	20.0
2	Minle	100°49′	38°27′	2,271	Farmland			
3	Sunan	99°37′	38°5′	2,312	Grassland			
4	Qilian	100°15′	38°11′	2,787	Grassland			
5	Yeniugou	99°35′	38°25′	3,320	Meadow			
6	Hulu-1	99°52.9′	38°16.1′	2,980	Grassland	TRwS 204 around a single Alter shield	70	25.2
7	Hulu-2	99°52.6′	38°14.9′	3,232	Shrub			
8	Hulu-3	99°52.2′	38°15.3′	3,382	Meadow			
9	Hulu-4	99°53.4′	38°13.9′	3,711	Swamp meadow			
10	Hulu-5	99°53.4′	38°13.3′	4,166	Talus moraine			
11	Hulu-6	99°52.4′	38°13.0′	4,484	Talus moraine			

(Aaltonen *et al.* 1993) and Mongolia (Zhang *et al.* 2004). A precipitation event of less than 0.10 mm is beyond the resolution of the CSPG and is recorded as trace precipitation. Ye *et al.* (2004) recommended assigning a value of 0.1 mm regardless of the number of trace observations per day. The wind-induced observation errors for rain, snow, and mixed precipitation are calibrated by using the precipitation measurement intercomparison (from 2009 to date) results from the study area (Chen *et al.* 2015).

The design of the TRwS 204 reduces its wetting, evaporation (the water is covered by anti-evaporation oil), and trace precipitation losses to near zero. Its wind-induced errors are calibrated with a Double-Fence Intercomparison Reference (DFIR) gauge with a Tretyakov-shielded CSPG ($CSPG_{DFIR}$) as the standard. Here the 'standard' $CSPG_{DFIR}$ is the sum of the measured $CSPG_{DFIR}$ data and its wetting, evaporation, and trace precipitation losses. The related calibration equations were reported by Zheng *et al.* (2017).

RESULTS AND DISCUSSION

AMP determining

As shown in Figure 2, four monthly AMPs may exist from 1,483 to 4,484 m according to the monthly precipitation versus altitude relationship between January 2014 and December 2016 (Figure 2). However, except for the 2,300-m AMP which is found in all months, the 2,800-m, 3,200-m and 4,200-m AMPs are only found in the most rainy months (Figure 2).

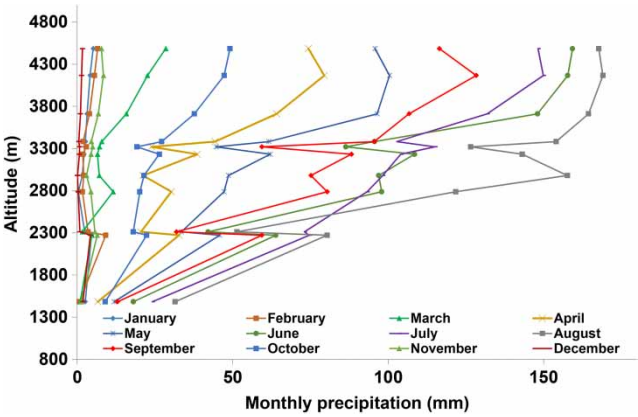

Figure 2 | Monthly precipitation varies with altitude from 1,483 to 4,484 m (from January 2014 to December 2016).

On a seasonal scale from 2014 to 2016, the 2,300-m AMP is found in all seasons, whereas the 2,800-m AMP only exists indistinctively in spring and autumn, and the 3,200-m and the 4,200-m AMPs appear in spring, summer, and autumn (Figure 3(a)). As a result, on a yearly scale, the 2,300-m, 3,200-m, and 4,200-m AMPs may exist, as shown in Figure 4.

Long-term observation data support the degree of reliability of AMPs and whereas only three years of data are available from 4,484 m, the recent observation data from 2010 to 2013 at another 10 stations from 1,483 m to 4,166 m (Figures 3(b) and 4), and historical data from 1960 to 2009 at five CMA stations below 3,350 m (Figures 3(c) and 4) are used for comprehensive analysis. As shown in Figures 3 and 4, the variations of these precipitation–altitude curves are similar in the lower regions. Thus, it can be deduced that precipitation also varies with altitude similarly in the higher areas in the past and the 4,200-m AMP should exist.

In winter, the 2,300-m AMP should exist because it has the maximum precipitation in the precipitation–altitude curves from 1960 to 2016 in Figure 3, although the snowfall is small in winter in the Qilian Mountains. However, the 2,300-m, 2,800-m, and 3,200-m AMPs should only be caused by the large precipitation difference between east and west in the Qilian Mountains in spring, summer, and autumn, and even on a yearly scale (Figures 3 and 4), because the four CMA stations (Minle, Sunan, Yeniugou, and Qilian) are distributed widely and separately from the A–B line (Figure 1) and the precipitation decreases largely from southeast to northwest in the Qilian Mountains (Zhang *et al.* 2008). As shown in Figures 3 and 4, the 2,300-m AMP is only caused by the large precipitation difference between Minle and Sunan stations. These two stations are located at similar elevations (2,271.5 and 2,311.7 m, respectively) but they are at a distance of about 112 km. The 2,800-m AMP is only evident in spring and summer and it is also caused by the small precipitation difference between Qilian and Hulu-1 (Figure 3(a)) or Yeniugou (Figure 3(c)) stations. The distance between Qilian and Hulu-1/Yeniugou stations is about 34/65 km. For the 3,200-m AMP, it is caused by lower precipitation at

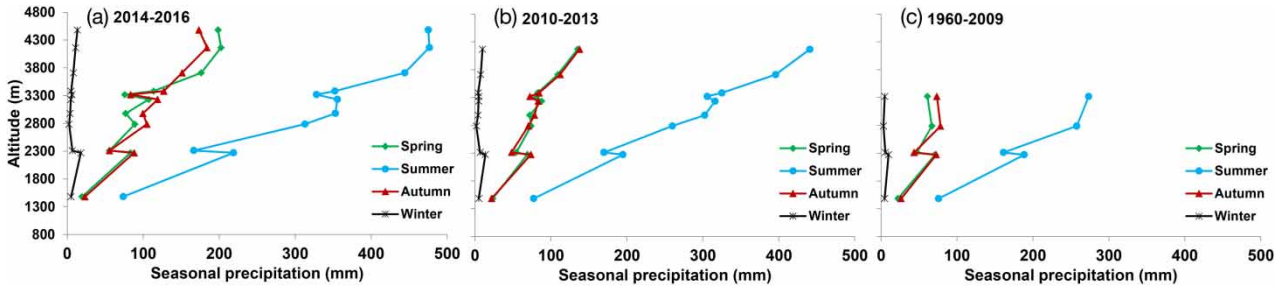

Figure 3 | Seasonal precipitation varies with altitude during 2014–2016 ((a) 1,483 m to 4,844 m), 2010–2013 ((b) 1,483 m to 4,166 m), and 1960–2009 ((c) 1,483 m to 3,320 m).

Yeniugou station in the western part of the study area, as shown in Figures 1, 3(a), and 4.

After removing the data at the four CMA stations (Minle, Sunan, Yeniugou, and Qilian), which are distributed widely and separately from the A–B line, the new precipitation–altitude curves are shown in Figure 5 by using the other seven station's data (including Zhangye and Hulu-1 to Hulu-6 stations) for the years 2014–2016. As shown in Figure 5, the 4,200-m AMP still exists, but there is no other AMP except an AMP at about 3,200 m in June and at about 3,000 m in August (Figure 5(a)), and a very obscure AMP at about 3,000 m in summer (Figure 5(b)). Because the AMP at about 3,000 m or 3,200 m is not very general, we are not sure whether it exists at the present time and needs to be observed intensively in the future.

Below and above the AMP, the lapse rates of the precipitation (Plaps) are different. The Plaps is also a very important factor in the interpolation procedures and hydrological modeling over the alpine regions. As summarized in Table 2, in the cold months (January, February, November, and December) and season (winter), there are three different Plaps from about 1,500 to 4,500 m (precipitation data are from all 11 stations shown in Table 1), since the precipitation–altitude curves are separated into three segments by the 2,300-m AMP (Figures 2 and 3(a)). In the warm months (from April to September except June) and seasons (spring, summer, and autumn), the Plaps are positive below the 4,200-m AMP but are negative above the AMP (precipitation data are from seven stations including Zhangye and six stations in the Hulu watershed). In the warm and cold transition months such as March and October, there is only one Plaps, from about 1,500 to 4,500 m (Table 2), because no AMP is monitored from 2014 to 2016 (Figure 5). In June, although there is an evident infection point at about 3,400 m (Figure 5(a)), the linear correlation is evident, resulting in one Plaps from about 1,500 to 4,500 m, in Table 2. In August, the infection point at about 3,000 m is also neglected. On yearly scale, the Plaps is about 281.9 and −43.1 mm/km below and above the 4,200-m AMP, respectively.

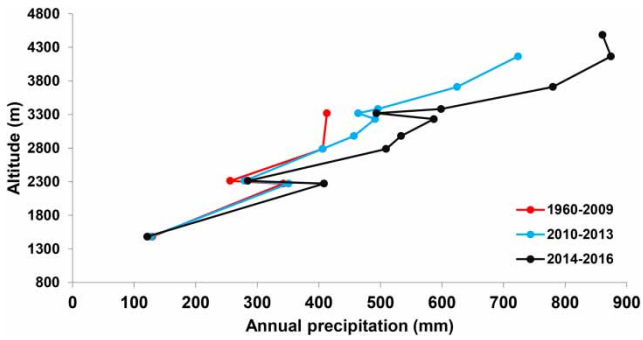

Figure 4 | Yearly precipitation varies with altitude.

According to the intercomparison between Figure 5 and Figures 2–4, the AMP is largely different when different combination of precipitation stations are used in this relatively small study area. Therefore, the determination of AMP has large uncertainties over the alpine regions where the distribution of precipitation is very complex. This result may explain why there is a great multiplicity of perspectives about AMP in the Qilian and other alpine regions, as described in the Introduction section.

In general, the evident AMP is sharply uplifted from about 2,300 m in winter to 4,200 m in spring, summer, and autumn. On a yearly scale, there is only one AMP, which appears at about 4,200 m with annual precipitation about 875 mm. The AMPs increase from the cold and dry season to the warm and wet season and therefore increase with precipitation at the northern flank of the Qilian Mountains.

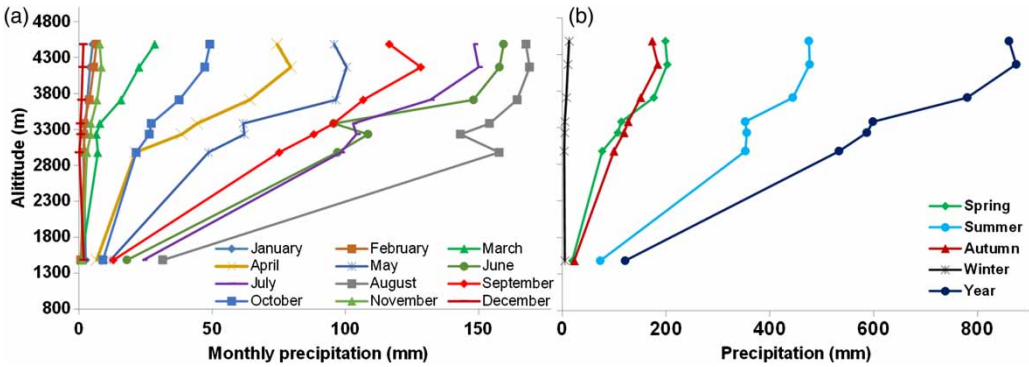

Figure 5 | Monthly (a), seasonal and annual (b) precipitation varies with altitude along the A–B line from 2014 to 2016.

Similarly, Erk (1887) noted a winter AMP of 700 m and a summertime increase to 1,600 m in the Bavarian Alps. In the southern Himalayas, Putkonen (2004) measured precipitation at 16 automatic stations from 1999 to 2001 at 500 to 4,400 m covering a 30×60-km area near Annapurna and reported that monsoon precipitation (June to September) has a clear maximum at about 3,000 m, whereas dry season precipitation (October to May) increases monotonically with altitude.

Causing factors

Barry (2008) noted that orographic precipitation involves air flow dynamics and physical processes in clouds. The key factors in the former are the depth of the air affected by topographically forced ascent and the strength of the uplift. The precipitation amounts might also be expected to decrease at higher elevations, but the vapor flux convergence, cloud-water

Table 2 | Lapse rate of precipitation (mm/km) for years 2014–2016 in the study area

Time	1,500–2,300 m	2,300–2,800 m	2,800–4,500 m	1,500–4,200 m	4,200–4,500 m	1,500–4,500 m
January	2.5	−6.5	2.2			
February	10.7	−10.1	3.1			
March						9.0
April				26.9	−16.1	
May				34.2	−14.7	
June						49.7
July				46.5	−5.3	
August				53.3	−4.2	
September				42.9	−37.2	
October						14.2
November	6.5	−3.4	3.0			
December	3.0	−4.9	0.9			
Spring				68.3	−12.4	
Summer				152.6	−4.7	
Autumn				59.0	−33.3	
Winter	16.3	−21.5	6.5			
Annual				281.9	−43.1	

In the cold months (from November to February) and winter, data from all the 11 stations in Table 1 are used, whereas in other months, seasons and on annual scale only data from seven stations are included (Zhangye and six stations in the Hulu watershed).

content, and vertical wind profile are the dominant influences.

Atmospheric circulation

As shown in Figure 6, a total of three circulations reach the Qilian Mountains (Wang *et al.* 2004; Xu *et al.* 2010): the plateau monsoon, the East Asian monsoon, and the westerly. The fluctuations in the intensity of these three circulations bring about a complex precipitation distribution on monthly, seasonal, and yearly scales. In general, the westerly predominates in both the summer and winter half-years. Browning (1985) noted that mountain effects on precipitation at mid-latitudes in the winter half-year are mainly modifications of extratropical cyclones. In the study area, the high-pressure weather system (Shule high and East Qilian high) predominates in winter (Tang 1963), leading to a sunny climate above the thermal inversion layer and a lower condensation level. When the forced wet plateau moisture is lifted by the westerly to the top of the inversion layer (about 2,200 m), it falls as snow (Lin 1995). Li *et al.* (2014) reported that 81% of snowfall is caused by the interaction between the dry and cold westerly and the warm and wet plateau moisture. This is a rational explanation for the 2,300-m AMP in the winter, shown in Figure 3.

During the summer half-year, the westerly provides the most water vapor from the Black Sea and the Caspian Sea to the study area (Wang *et al.* 2004; Zhao *et al.* 2011). An atmospheric depression (the Heihe depression) forms near 40 °N latitude (Tang 1963; Lin 1995). In the westerly in middle latitudes, the wind speed typically increases with height. Only a small fraction of the increase can be attributed to an increased frequency of days with precipitation (Barry 2008). Both the depression and the westerly jet at 200 hpa prompt the large-scale forced ascent of air (Cheng *et al.* 2007), which leads to more precipitation in the mountains.

Synoptic scale convection and topographical enhanced uplifting

During the summer half-year, the westerly predominates in the study area. The wind speed increase with height more than compensates for the vertical decrease in the moisture content up to at least 700 hpa (Barry 2008). The large-scale forced ascent of air leads to lifting condensation. This

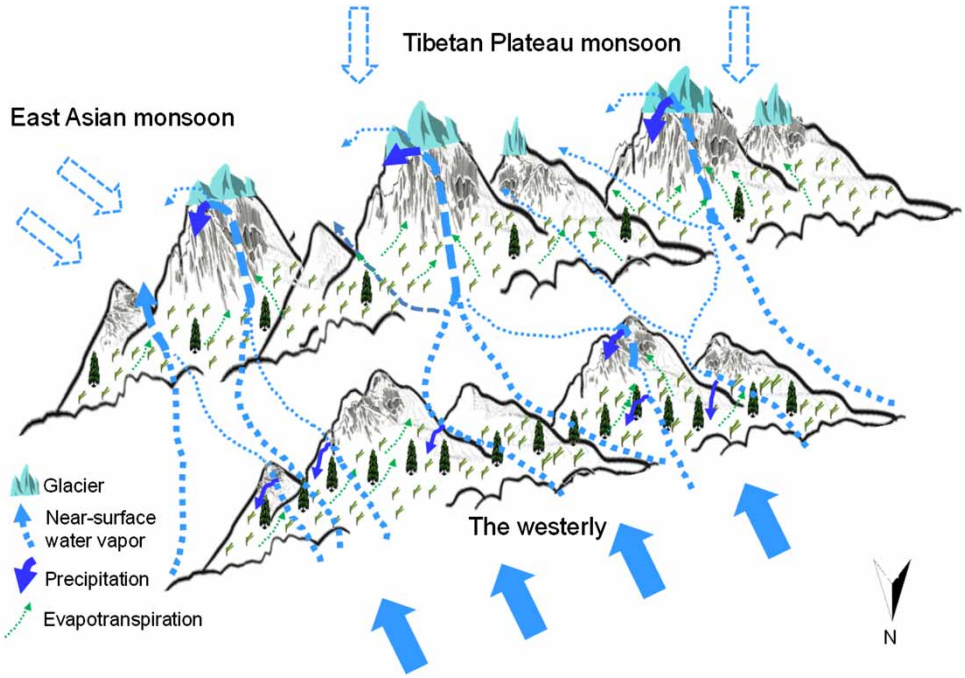

Figure 6 | Schematic diagram of the near-surface moisture movement forced by terrain uplifting during the wet season when the westerly reaches the study area.

ascent intensifies the general vertical motion in a cyclonic system and enhances conditional instability and shower processes. The synoptic scale uplift or convective instability is the main reason that small towering cumulus clouds are often observed in the rainy season in the study area, especially near the high mountain summit. These towering cumulus clouds generated by thermal convection and valley wind effects often cause thunder showers in the afternoon and evening, mainly between 16:00 and 06:00 according to the measurements in the Hulu watershed, and especially at 16:00, 20:00, and 22:00. As a result, local precipitation is often recorded, especially in the higher areas. According to the precipitation data recorded by the six automatic weighted rain and snow gauges (Hulu-1 to Hulu-6 in Figure 1 and Table 1) in the Hulu watershed, more than 120 precipitation events occurred above 3,700 m (Hulu-4 to Hulu-6), whereas only 96 events were recorded at 2,980 m (Hulu-1; Figure 7) in 2015, even though these six gauges are separated by only about 5 km in linear distance (Figure 1). Here, the definition of 'event' follows that of Robinson & Henderson (1992): an event is a period of continuously recorded precipitation separated from other such periods by a dry interval of 2 hours or more. The choice of the 2-hour separation interval has a slight influence on the climatological frequency distributions, but it maintains a distinction between convective and cyclonic systems. Local precipitation induced by synoptic scale uplift or convective instability makes certain contributions to the greater precipitation in higher regions. Barry (2008) noted that mountain effects on precipitation in the middle latitudes involve the modification of

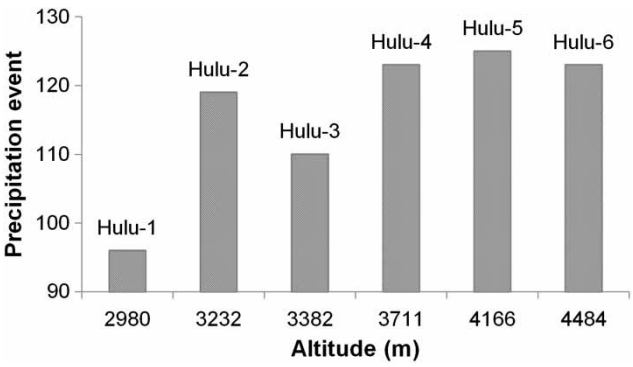

Figure 7 | Precipitation events in 2015 in the Hulu watershed.

extratropical cyclones during the winter half-year (Browning 1985) and convective systems in summer (Cotton *et al.* 1983). Topographical enhancement of precipitation is most commonly caused by synoptic scale uplift or convective instability. Related meteorological measurements also show lower temperatures and greater precipitation above 3,700 m, where the moisture condenses more easily (Figure 8).

In brief, more water vapor is brought to the region by the westerly air current, and the uplifting mechanism develops due to the topography and synoptic convection during the summer half-year. During summer, the warm and unstable air current contains the most water vapor during the year, which is brought by the westerly air current, the East Asian summer monsoon, and local evaporation (Figure 6). The summer convergent air current of the Tibetan Plateau monsoon makes the warm and wet air current move from the north toward the Qilian Mountains, and the enhanced uplifting by the mountains produces increasing precipitation with altitude, thus forming the 4,200-m AMP.

Mountain topography

The vertical motion induced by the terrain is determined by the air mass stability, wind speed and direction, and the topography and landforms (Barry 2008). As shown in Figure 6, when the lower moisture is forced by the westerly to ascend from the northern lowland (see Figure 1(a)) to the southern Qilian Mountains, it climbs over several parallel mountains and passes through many valleys. The airflow is forced to ascend and descend several times, which causes several AMPs (Lin 1995). This is part of the reason why there is an AMP at about 3,650 m in the Sidalong region, reported by Chang *et al.* (2002). Carruthers & Choularton (1983) even reported that for wide hills with half-widths of 20 km or more, the AMP occurs not on the upwind side, but at the summit or in the lee of narrow hills due to wind drift.

Alpert (1986) noted that the AMP is always shifted to lower levels than the point of the steepest slope. As shown in Figure 1(b), the slope is relatively gentle from 4,100 to 4,300 m, whereas the average slope is steeper than 65° from 4,500 to 4,800 m. The steep terrain contributes somewhat to the formation of the 4,200-m AMP. Similarly, the

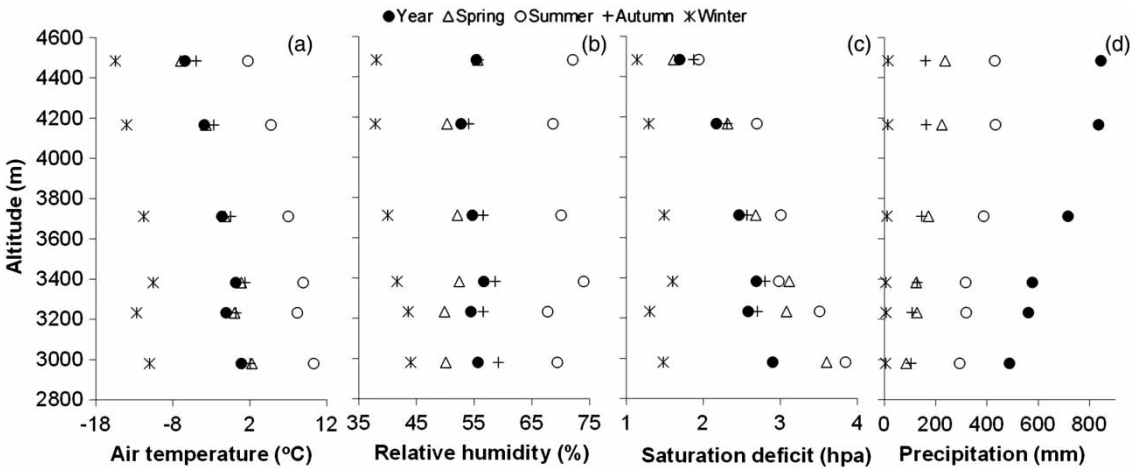

Figure 8 | Seasonal and annual air temperature (a), relative humidity (b), saturation deficit (c), and precipitation (d) vary with altitude in 2015 in the Hulu watershed.

3,650-m AMP, reported by Chang *et al.* (2002), may also be partly caused by the steep terrain from 3,700 m to the 4,200 m summit at the Sidalong site (Figure 1(d)).

In addition, large, deep valleys establish their own wind systems that can cause very different distributions of precipitation (Barry 2008). In these cases, the local valley breeze during the day and the mountain breeze at night contribute to the formation of AMP during the summer half-year. The different wind systems could cause different precipitation distributions. As shown in Figures 3(a), 4, and 7, the Hulu-5 gauge recorded the most precipitation and the most precipitation events at 4,166 m, leading to the 4,200-m AMP in the study area, especially during the wet season (Figures 2 and 3(a)). According to the wind field data at 08:30 and 15:30 on July 14, 2015, in the small Hulu watershed, the local wind field is very complex, and one of the convergence areas is exactly located at about 4,200 m near the Hulu-5 station (Figure 9).

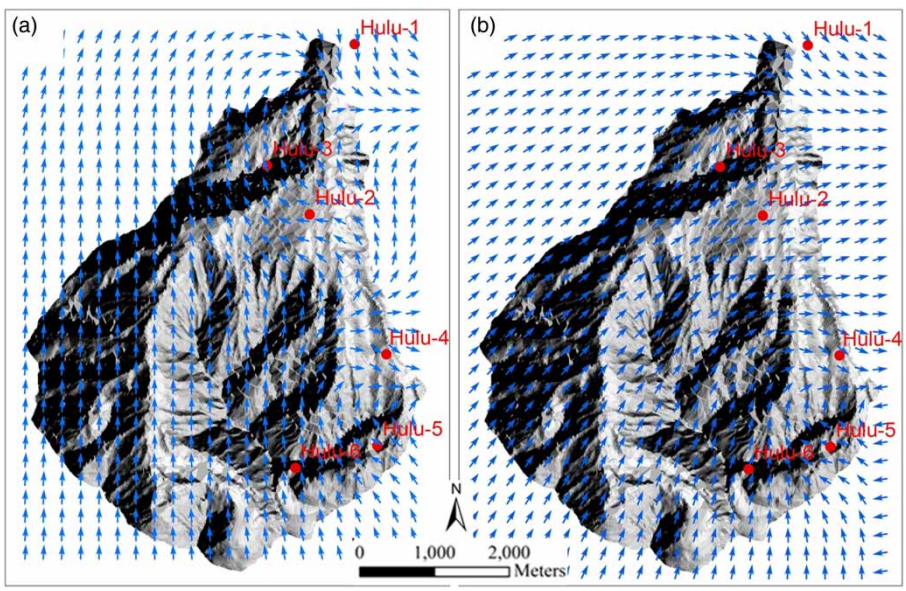

Figure 9 | Wind field at 1.5 m height at 8:30 (a) and 15:30 (b) on July 14, 2015, in the Hulu watershed. Wind direction is interpolated with data at Hulu-1–6 stations.

Land cover

As described in the Data and methods section, vertical landscape belts are obvious in the study area. The water cycle and energy balance of this land cover modifies the local precipitation distribution. The isotope results have shown that the local moisture is a partial source of the precipitation in the study area (Zhao *et al.* 2011).

There are 2,684 glaciers in the Qilian Mountains (Guo *et al.* 2015). Bai & Yu (1986) have reported that the air temperature is much colder than outside the area due to the high albedo and 'cold source' effects of the large glaciers in West China. Recent data from the Koxcar glacier in the Tien Mountains (with an approximate area of 85 km^2; Han *et al.* 2006) also show that the mean air temperature is 1.2 °C colder on the glacier (80°07′29.9″E, 41°48′40.0″N; 4,021 m) than that outside the area (80°06′39.0″E, 41°47′57.0″N; 3,956 m) from November 2007 to June 2008 (Figure 10(a)). This difference is much greater than the normal lapse rate. During the same period, the mean relative humidity was 1.7% wetter on the glacier than outside it (Figure 10(b)). According to the numerical simulation results (Truman 1987; Hu 1987) and theoretical analysis (Shen & Liang 2004), more precipitation would occur on the large glacier than in the surrounding area.

On a small glacier with an area of about 2.5 km^2 in the Qilian Mountains (the Qiyi glacier in Figure 1(a); half sunny slope), Wang *et al.* (2009) reported that the air temperature is lower than in the surrounding area, but the relative humidity is similar to that outside. Their results showed that the 4,600-m AMP (about 4,510 to 4,670 m) lies near the rear of the glacier tongue where the cold glacier wind (fall wind) and the warm upslope wind often converge, leading to more precipitation near the glacier terminus in the wet season. This result is in agreement with those of studies on a large glacier in the Mexican Plateau (Lauscher 1976) and on Mt. Tomur in China (Lin 1995).

Coincidentally, the glacier terminus is located at about 4,200 to 4,300 m (Guo *et al.* 2015) near the 4,200-m AMP on the northern slope of the Qilian Mountains. However, among the 2,684 glaciers in the Qilian Mountains, 85.7% are smaller than 1.0 km^2 and 99.9% are smaller than

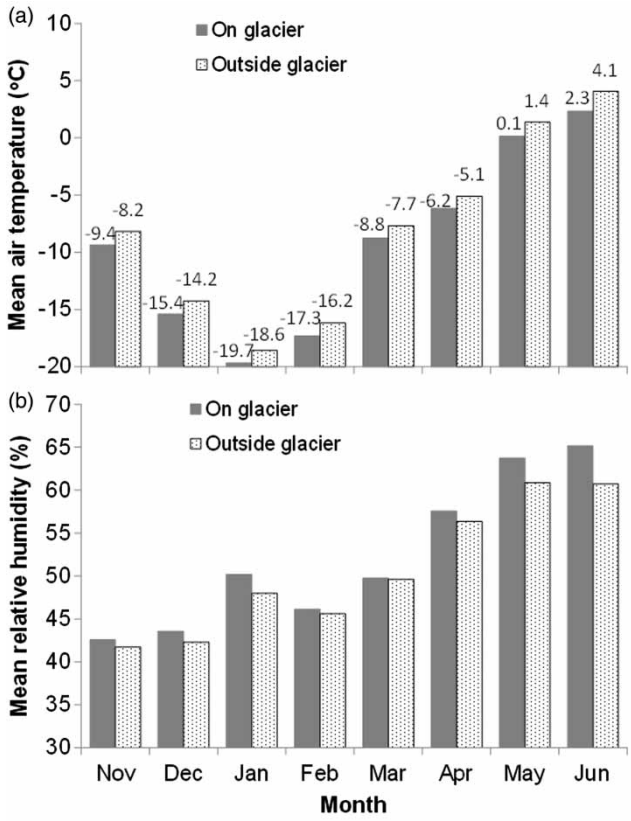

Figure 10 | Monthly mean air temperature (a) and relative humidity (b) from November 2007 to June 2008 on and outside Koxcar glacier in Tien Mountains.

2.0 km^2. There are five small glaciers within an area of about 1.5 km^2 near the Hulu-5 station in the Hulu watershed. As shown in Figure 9, one of the convergence areas is located at about 4,200 m. It should be determined whether the 4,200-m AMP is partly caused by these small glaciers or by the valley and mountain breezes.

In addition, the Qilian Mountains include 5,265 km^2 of forests, including *Picea crassifolia*, *Sabina przewalskii*, and various kinds of shrubs (Figure 1(c)). According to the measured data from 2003 to 2006 from the Dayekou station (100°17′E, 38°24′N; 2,750 m), the monthly air temperature is lower in the *P. crassifolia* forest than that outside except during March, April, and September (Figure 11(a)), leading to a 0.24 °C decrease in the annual value, whereas the annual mean relative humidity is 9.4% higher in the forest than outside the forest (Figure 11(b)). Recent results have shown annual evapotranspiration of about 400 to 500 mm in the *P. crassifolia* forest and the adjacent grassland (e.g.,

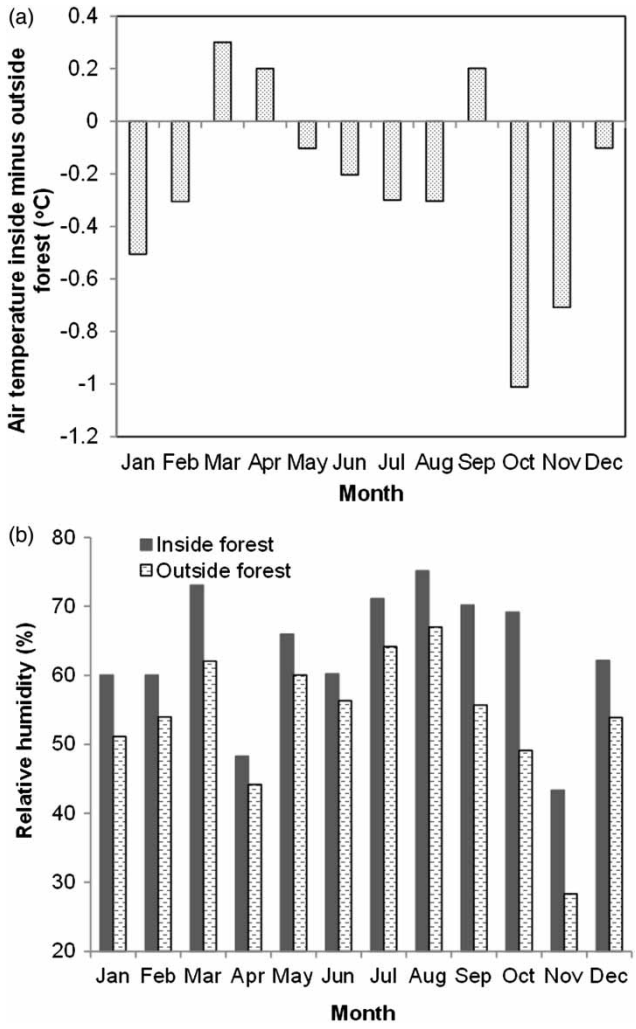

Figure 11 | Monthly mean air temperature difference (a) and relative humidity (b) in and out of the *Picea crassifolia* forest from 2003 to 2006 in the study area.

He *et al.* 2012; Chang *et al.* 2014), and part of the local moisture would undergo evapotranspiration (Figure 7) according to the isotope result (Zhao *et al.* 2011). Burns (1953) explained that the AMP is the combined result of two opposing effects; one is due to the enhanced moisture condensation as the barrier height increases, and the other is due to the exponential reduction in the quantity of available moisture as the elevation increases. Hu (1987) simulated this kind of 'cold and wet island effect' and concluded that it would be in favor of condensation. It may contribute to the large precipitation in August in Figure 2 and in summer in Figure 3(a) at about 3,100 m near the upper limit of *P. crassifolia* forest.

As described above, in the summer half-year, more water vapor is carried to the area by the westerly current and the East Asian monsoon, and local evaporation also produces water vapor. The relatively abundant water vapor is transported by the Tibet summer monsoon northward to the Qilian Mountains. The synoptic scale convection and topographically enhanced uplifting then generate more precipitation and cause the formation of AMP at the higher areas at the northern flank of the Qilian Mountains. The combination of the local wind field caused by mountain and valley breezes, the front steepest terrain, and glacier cover causes the formation of AMP at about 4,200 m in the study area.

However, the factor of the front steepest terrain should be the main causing factor, since the three discovered AMPs (4,200-m AMP in Hulu watershed, 4,600-m AMP on Qiyi glacier, and 3,650 m at Sidalong site; Figure 1(a)) are all located at lower levels than the point of the steepest slope at the north flank of the Qilian Mountains. In addition, the ratio of the annual AMP to the altitude of the mountain top (MaxA) is about 0.88 (AMP/MaxA = 4,200/4,800 ≅ 0.88) in the study area. Similarly, in the adjacent regions at the north flank of the Qilian Mountains, this ratio is about 0.89 (4,600/5,150) and 0.87 (3,650/4,200) in the Qiyi glacier watershed (Wang *et al.* 2009) and Sidalong watershed (Chang *et al.* 2002; Figure 1(a)), respectively. Is the AMP roughly equal to seven-eighths of the MaxA at the north flank of the Qilian Mountains? Further studies are needed. Generally, the terrain is much steeper above than below the altitude of the seven-eighths of the MaxA at the north flank of the Qilian Mountains.

As noted by Barry (2008), the effect of altitude on the vertical distribution of precipitation in mountainous areas is highly variable in different geographic locations. High-resolution fields of precipitation in mountainous areas are almost impossible to obtain from gauge data, given the typical network densities, even with sophisticated interpolation procedures. Therefore, measurements on small and large spatial scales, empirical models, regional or mesoscale atmosphere modeling, and remote sensing are all important and should be combined to increase our knowledge of the distribution of precipitation in alpine regions.

CONCLUSIONS

One AMP exists at about 2,300 m in winter, and another is located at about 4,200 m in other seasons and on a yearly scale with annual precipitation about 875 mm at the northern flank of the Qilian Mountains. The AMPs increase from the cold and dry season to the warm and wet season and therefore increase with precipitation.

The large scale atmosphere circulation, synoptic scale convective uplift, mountain shape and relief, and the land covers of forest and glaciers are analyzed to understand the formation mechanisms of AMPs at the northern flank of the Qilian Mountains. The cold, dry, high-pressure circulation system leads to the 2,300-m AMP in winter. In the summer half-year, more water vapor is carried to the area by the westerly current and the East Asian monsoon, and local evaporation also produces water vapor. The relatively abundant water vapor is transported by the Tibet summer monsoon northward to the Qilian Mountains. The synoptic scale convection and topographically enhanced uplifting then generate more precipitation and cause the formation of AMP in the higher areas at the northern flank of the Qilian Mountains. The front steepest terrain is the primary factor causing the formation of AMP at about 4,200 m in the study area. The annual AMP may be roughly equal to seven-eighths of the altitude at the mountain top on the northern flank of the Qilian Mountains.

This study indicates that the variations in mountain AMP and its mechanisms are very complex, and our understanding and knowledge are still preliminary. Further field experimental measurements and studies should be carried out on different spatial scales. Regional mathematical models should be developed in combination with the regional and mesoscale atmosphere models and remote sensing methods to further understand the spatial and temporal distribution of mountain precipitation and its AMPs.

ACKNOWLEDGEMENTS

This study was supported primarily by the National Basic Research Program of China (2013CBA01806) and the National Natural Sciences Foundation of China (41671029 and 41690141).

REFERENCES

Aaltonen, A., Elomaa, E., Tuominen, A. & Valkovuori, P. 1993 Measurement of precipitation. In: *Proceedings of the Symposium on Precipitation and Evaporation* (B. Sevruk & M. Lapin, eds). Slovak Hydrometeorological Institute and Swiss Federal Institute of Technology, Bratislava, Slovakia, pp. 42–46.

Ahrens, B. 2006 Distance in spatial interpolation of daily rain gauge data. *Hydrol. Earth Syst. Sci.* **10**, 197–208.

Aizen, V. B., Aizen, E. M. & Melack, J. M. 1996 Precipitation, melt and runoff in the northern Tien Shan. *J. Hydrol.* **186**, 229–251.

Akkiraz, M. S., Akgün, F., Utescher, A. A., Bruch, T. & Mosbrugger, V. 2011 Precipitation gradients during the Miocene in western and central Turkey as quantified from pollen data. *Palaeogeogr. Palaeocl.* **304**, 276–290.

Alpert, P. 1986 Mesoscale indexing of the distribution of orographic precipitation over high mountains. *J. Clim. Appl. Meteorol.* **25**, 532–545.

Bai, C. & Yu, X. 1986 Energy exchange and its influence factors on mountain glaciers in west China. *Ann. Glaciol.* **6**, 154–157.

Barry, G. R. 1981 *Mountain Weather and Climate.* Methuen & Co., London and New York.

Barry, G. R. 2008 *Mountain Weather and Climate,* 3rd edn. Cambridge University Press, Cambridge.

Browning, K. A. 1985 Conceptual models of precipitation systems. *Wea. Forecasting* **1**, 23–41.

Burns, J. I. 1953 Small-scale topographic effects on precipitation distribution in San Dimas experimental forest. *Trans. Amer. Geophys. Union* **34**, 761–768.

Carruthers, D. J. & Choularton, T. W. 1983 A model of the seeder-feeder mechanism of orographic rain including stratification and wind-drift effects. *Q. J. R. Met. Soc.* **109**, 575–588.

Chang, X., Zhao, A., Wang, J., Chang, Z. & Jin, B. 2002 Precipitation characteristic and interception of forest in Qilian Mountain. *Plateau Meteorol.* **21**, 274–280.

Chang, X., Zhao, W., Liu, H., Wei, X., Liu, B. & He, Z. 2014 Qinghai spruce (*Picea crassifolia*) forest transpiration and canopy conductance in the upper heihe river basin of arid northwestern China. *Agr. Forest Meteorol.* **198–199**, 209–220.

Chen, R., Song, Y., Kang, E., Han, C., Liu, J., Yang, Y., Qing, W. & Liu, Z. 2014 A cryosphere-hydrology observation system in a small alpine watershed in the qilian mountains of China and its meteorological gradient. *Arct. Antarct. Alp. Res.* **46** (2), 505–523.

Chen, R., Liu, J., Kang, E., Yang, Y., Han, C., Liu, Z., Song, Y., Qing, W. & Zhu, P. 2015 Precipitation measurement intercomparison in the qilian mountains, northeastern Tibetan Plateau. *Cryosphere* **9**, 1995–2008.

Cheng, P., Tao, J., Zhang, X. & Yang, X. 2007 Influences of upper-level westerly jet on precipitation over Qilian Mountain. *Meteorol. Sci. Tech.* **35**, 489–494.

Cotton, W. R., George, R. L., Wetzel, P. J. & McAnelly, R. L. 1983 A long-lived mesoscale convective complex. part I: the

mountain generated component. *Mon. Weather Rev.* **111**, 1897–1918.

Ding, L., Kang, X. 1985 Climatic condition of glacier formation and its impacts on the glacier features in Qilian Mountains. In: *Memoirs of Lanzhou Institute of Glaciology and Geocryology* (Lanzhou Institute of Glaciology and Geocryology, ed.). Science Press, Beijing, No. 5, 9–15.

Ding, Y., Ye, B. & Zhou, W. 1999 Temporal and spatial precipitation distribution in the Heihe catchment, Northwest China, during the past 40 a. *J. Glaciol. Geocryol.* **21** (1), 42–48.

Erk, F. 1887 Die vertikale verteilung und die maimalzone des neiderschlags am nordhange der bayrischen alpien im zeitraum November 1883 bis November 1885. *Met. Zeit.* **4**, 55–69.

Fu, B. 1992 The effects of topography and elevation on precipitation. *Acta Geogr. Sin.* **47**, 302–314.

Gao, H., He, X., Ye, B. & Pu, J. 2012 Modeling the runoff and glacier mass balance in a small watershed on the central Tibetan plateau, China, from 1955 to 2008. *Hydrol. Process.* **26** (11), 1593–1603.

Gao, H., Ding, Y., Zhao, Q., Hrachowitz, M. & Savenije, H. H. G. 2017 The importance of aspect for modelling the hydrological response in a glacier catchment in Central Asia. *Hydrol. Process.* **31** (16), 2842–2859.

Goodison, B. E., Louie, B. P. Y. T. & Yang, D. 1998 *WMO Solid Precipitation Measurement Intercomparison: Final Report, Instrum. and Obs. Methods Rep. 67/Tech. Doc. 872*, World Meteorological Organization, Geneva, Switzerland.

Guo, W., Liu, S., Xu, J., Wu, L., Shangguan, D., Yao, X., Wei, J., Bao, W., Yu, P., Liu, Q. & Jiang, Z. 2015 The second Chinese glacier inventory: data, methods and results. *J. Glaciol.* **61** (226), 357–372.

Han, H., Ding, Y. & Liu, S. 2006 A simple model to estimate ice ablation under a thick debris layer. *J. Glaciol.* **52**, 528–536.

He, Z., Zhao, W., Liu, H. & Tang, Z. 2012 Effect of forest on annual water yield in the mountains of an arid inland river basin: a case study in the pailugou catchment on northwestern China's qilian mountains. *Hydrol. Process.* **26**, 613–621.

Hu, Y. 1987 A result of numerical experiment on weaker cold island. *Plateau Meteorol.* **6**, 1–8.

Kotlyakov, V. M. & Krenke, A. N. 1982 Investigations of the hydrological conditions of alpine region by glaciological methods. In: *Hydrological Aspects of Alpine and High-Mountain Areas. Exeter Symposium*, IAHS Publ., 138, pp. 31–42.

Kou, Y. & Su, Z. 1981 Variation of precipitation with altitude and its impacts on recharge of glaciers in Tuomuer. *Chin. Sci. Bull.* **26** (2), 113–115.

Lauscher, F. 1976 Weltweite typen der hohenabhangigkeit des niederschlags. *Wetteru. Leben* **28**, 80–90.

Li, J. 1976 About distribution of the alpine precipitation. *Meteorol. Sci. Tech.* **4** (8), 23–25.

Li, J. 1982 Characteristics of profiles of alpine precipitation. *Xinjiang Meteorol.* **27** (3), 3–5.

Li, L. P., Chen, L., Wang, R. Z. & Yin, Y. C. 2014 Analysis of winter snowfall east of the Hexi Corridor. *Resource Science* **36**, 0182–0190.

Lin, Z. 1995 *Climatology of Orographic Precipitation.* Science Press, Beijing.

Marquínez, J., Lastra, J. & García, P. 2003 Estimation models for precipitation in mountainous regions: the use of GIS and multivariate analysis. *J. Hydrol.* **270**, 1–11.

Mueller, B. & Seneviratne, S. I. 2014 Systematic land climate and evaporation biases in CMPI5 simulations. *Geophys. Res. Lett.* **41**, 128–134.

Prat, O. P. & Barros, A. P. 2010 Ground observations to characterize the spatial gradients and vertical structure of orographic precipitation: experiments in the inner region of the great smoky mountains. *J. Hydrol.* **391**, 141–156.

Putkonen, J. K. 2004 Continuous snow and rain data at 500 to 4400 m altitude near Annapurna, Nepal, 1999–2001. *Arct. Antarct. Alp. Res.* **36** (2), 244–248.

Robinson, J. P. & Henderson, G. K. 1992 Precipitation events in the southeast United States of America. *Int. J. Climatol.* **12**, 701–720.

Roe, G. H. 2005 Orographic precipitation. *Annu. Rev. Earth Planet. Sci.* **33**, 645–671.

Rubel, F. & Rudolf, B. 2001 Global daily precipitation estimates proved over the European Alps. *Meteorol. Zeit.* **10**, 403–414.

Rumney, G. R. 1968 *Climatology and the World's Climates.* Macmillan, London.

Sarker, P. R. 1966 A dynamical model of orographic rainfall. *Mon. Weather Rev.* **94**, 52–72.

Sevruk, B. & Mieglitz, K. 2002 The effect of topography, season and weather situation on daily precipitation gradients in 60 Swiss valleys. *Water Sci. Technol.* **45** (2), 41–48.

Sevruk, B. & Nevenic, M. 1998 The geography and topography effects on the areal pattern of precipitation in a small pre-alpine basin. *Water Sci. Technol.* **37** (11), 163–170.

Shen, Z. 1975 Characteristics of precipitation in Mount Qomolangma. In: *Scientific Report of the Investigation on Mt Qomolangma (1966–1968), Meteorology and Solar Radiation.* (Xizang Science Expedition Team of the Chinese Academy of Sciences ed.), Science Press, Beijing, pp. 11–20.

Shen, Y. & Liang, H. 2004 High precipitation in glacial region of high mountains in High Asia: possible cause. *J. Glaciol. Geocryol.* **26** (6), 806–809.

Sugiura, K., Yang, D. & Ohata, T. 2003 Systematic error aspects of gauge-measured solid precipitation in the Arctic, barrow, Alaska. *Geophys. Res. Lett.* **30**, 1192.

Tang, M. 1963 Pressure system in the mountainous region of west gansu. *Acta Meteorol. Sin.* **33**, 175–188.

Tang, M. 1985 The distribution of precipitation in mountain Qilian (Nanshan). *Acta Geog. Sin.* **40** (4), 323–332.

Thomas, A. 1997 The climate of the Gongga Shan range, Sichuan province, P R China. *Arct. Antarct. Alp. Res.* **29**, 226–232.

Truman, A. P. 1987 Thermal influences on airflow in mountainous terrain. *Prog. Phys. Geogr.* **11**, 183–206.

Wang, K., Cheng, G., Xiao, H. & Jiang, H. 2004 The westerly fluctuation and water vapor transport over the Qilian-Heihe valley. *Sci. China (Series D)* **47** (SI), 32–38.

Wang, N., He, J., Jiang, X., Song, G., Pu, J., Wu, X. & Chen, L. 2009 Study on the zone of maximum precipitation in the north slopes of the central Qilian mountains. *J. Glaciol. Geocryol.* **31** (3), 395–403.

Ward, E., Buytaert, W., Peaver, L. & Wheater, H. 2011 Evaluation of precipitation products over complex mountainous terrain. A water resources perspective. *Adv. Water Resour.* **34**, 1222–1231.

Wulf, H., Bookhagen, B. & Scherler, D. 2010 Seasonal precipitation gradients and their impact on fluvial sediment flux in the Northwest Himalaya. *Geomorphology* **118**, 13–21.

Xu, C.-Y. & Singh, V. P. 1998 A review on monthly water balance models for water resources investigations. *Water. Resour. Manage.* **12**, 20–50. doi: 10.1023/A:1007916816469.

Xu, J., Wang, K., Jiang, H., Li, Z., Sun, J., Luo, X. & Zhu, Q. 2010 A numerical simulation of the effects of westerly and monsoon on precipitation in the Heihe River basin. *J. Glaciol. Geocryol.* **32** (3), 489–496.

Xu, R., Tian, F. Q., Yang, L., Hu, H. C., Lu, H. & Hou, A. Z. 2017 Ground validation of GPM IMERG and TRMM 3b42v7 rainfall products over southern Tibetan plateau based on a high-density rain gauge network. *J. Geophys. Res.* **122**. doi: 10.1002/2016JD025418.

Yang, D. 1988 *Research on Analysis and Correction of Systematic Errors in Precipitation Measurement in Urumqi River Basin, Tianshan*. PhD thesis, Lanzhou Institute of Glaciology and Geocryology, Chinese Academy of Sciences, Lanzhou, China.

Yang, D., Shi, Y., Kang, E., Zhang, Y. & Yang, X. 1991 Results of solid precipitation measurement intercomparison in the alpine area of Urumqi River basin. *Chin. Sci. Bull.* **36**, 1105–1109.

Yang, Z., Liu, X., Zeng, Q. & Chen, Z. 2000 *Hydrology in Cold Regions of China*. Science Press, Beijing.

Ye, B., Yang, D., Ding, Y., Han, T. & Koike, T. 2004 A bias-corrected precipitation climatology for China. *J. Hydrometeorol.* **5**, 1147–1160.

Zhang, J. & Deng, Z. 1987 *An Introduction to the Precipitation in Xinjiang*. China Meteorological Press, Beijing.

Zhang, Y., Ohata, T., Yang, D. & Davaa, G. 2004 Bias correction of daily precipitation measurements for Mongolia. *Hydrol. Process.* **18**, 2991–3005.

Zhang, Q., Yu, Y. & Zhang, J. 2008 Characteristics of water cycle in the Qilian Mountains and the oases in Hexi inland river basins. *J. Glaciol. Geocryol.* **30** (6), 907–913.

Zhao, L., Yin, L., Xiao, H., Cheng, G., Zhou, M., Yang, Y., Li, C. & Zhou, J. 2011 Isotopic evidence for the moisture origin and composition of surface runoff in the headwaters of the Heihe river basin. *Chin. Sci. Bull.* **56**, 406–416.

Zheng, Q., Chen, R., Han, C., Liu, J., Song, Y., Liu, Z., Yang, Y., Wang, L., Wang, X., Liu, X., Guo, S. & Liu, G. 2017 Correcting precipitation measurements of TRwS204 in the Qilian Mountains, China. *Hydrol. Earth Syst. Sci. Discuss.* doi:10.5194/hess-2017-8.

First received 16 July 2017; accepted in revised form 23 January 2018. Available online 19 February 2018